

See discussions, stats, and author profiles for this publication at: <https://www.researchgate.net/publication/349038900>

(Preprint) AAS 21-208 AUTONOMOUS SPACECRAFT OBSTACLE AVOIDANCE AND TRAJECTORY TRACKING IN DENSE DEBRIS FIELD

Conference Paper · February 2021

CITATIONS

0

READS

130

4 authors, including:



Madhur Tiwari

Florida Institute of Technology

9 PUBLICATIONS 1 CITATION

[SEE PROFILE](#)



David Zuehlke

Embry-Riddle Aeronautical University

10 PUBLICATIONS 11 CITATIONS

[SEE PROFILE](#)

Some of the authors of this publication are also working on these related projects:



Autonomous Spacecraft Missions Near Asteroid [View project](#)



Optical Orbit Determination and Space Surveillance Research [View project](#)

AUTONOMOUS SPACECRAFT OBSTACLE AVOIDANCE AND TRAJECTORY TRACKING IN DENSE DEBRIS FIELD

Madhur Tiwari*, David Zuehlke†, Troy Henderson‡, and Richard J. Prazenica§

In this paper, we implement an autonomous path planning technique using artificial potential functions paired with a direct adaptive controller for spacecraft trajectory tracking through a dense debris field. The debris field is modeled as fixed debris and the spacecraft is modeled using relative orbital dynamics with disturbances. The spacecraft is assumed to be in proximity to a dense debris field that it must navigate through to reach a goal destination. Obstacle avoidance trajectories are generated using model independent artificial potential functions that rely only on the position measurements of the debris with respect to the spacecraft. A direct adaptive controller is implemented to track generated trajectories because it can achieve robust tracking in the presence of model and path uncertainties.

INTRODUCTION

The ever increasing population of orbiting debris objects poses significant risk for spacecraft collisions. Spacecraft proximity operations in the presence of debris objects require robust obstacle avoidance to prevent collisions. Space debris is rising at a rapid rate due to increased interest in space missions, decommissioned or non-cooperative satellites, anti-satellite tests and accidental collisions between spacecrafts. Although significant amounts of space debris are cataloged in the US Satellite Catalog, it is the smaller and uncatalogued space debris that pose the most threat to spacecraft in orbit.¹ Currently, most of the debris collision avoidance is performed manually using ground in loop techniques. However, with the rise of mega constellations such as SpaceX's StarLink constellation, it is necessary to develop technologies to autonomously perform these maneuvers for safety and less reliance on ground control.

Several researchers are focusing on developing techniques for collision avoidance. In a recent paper,² authors present a novel technique to avoid debris using attitude control in low earth orbit (LEO) by changing the semi-major axis of the orbit. Another approach has been to use aerodynamic drag for collision avoidance.³

Most obstacle collision avoidance techniques are dependent on the system model and require prior knowledge of the obstacles and do not focus on avoidance with sudden unknown obstacles. Collision avoidance using Artificial Potential Fields (APF) is well studied formulation used for realtime

*PhD Candidate, Embry-Riddle Aeronautical University, Department of Aerospace Engineering, Daytona Beach, Florida, USA.

†PhD Candidate, Aerospace Engineering, Embry-Riddle Aeronautical University, 1 Aerospace Blvd., Daytona Beach Florida

‡Assistant Professor, Embry-Riddle Aeronautical University, Department of Aerospace Engineering, Daytona Beach, Florida, USA.

§Associate Professor, Embry-Riddle Aeronautical University, Department of Aerospace Engineering, Daytona Beach, Florida, USA.

robot path planning. The path planning algorithm used here does not require system model information and can be used for sudden and unknown obstacles using sensor information only. Artificial potential functions (APFs) have seen extensive use in robotics and navigation problems applied to obstacle avoidance.⁴⁻⁷ Combining APFs with sliding mode control (SMC), provides a robust control algorithm for reaching a goal point while avoiding obstacles. APFs and SMC are used for the case of static obstacles and reaching a goal position using a 6 Degree-of-Freedom (DOF) relative motion simulation.⁵ Way-point navigation around obstacles of varying sizes were considered and successfully navigated around. Another work⁸ applied a similar control method for the problem of spacecraft rendezvous with a constrained motion path. The motion constraint consideration provides collision avoidance with “forbidden zones” during a rendezvous or docking maneuver. An example of such a zone to avoid would be avoiding solar panels of the target spacecraft while docking with zero relative pose error. A combined optimal control methods with APFs and SMC are used to achieve an optimal trajectory tracking method with obstacle avoidance and guaranteed convergence to a goal point.⁹

One significant drawback of these control methods has been the assumption of relatively few, static obstacles. Also, the artificial potential functions and force fields were written directly into the control laws and system dynamics, adding complexity to the control algorithms and system dynamics. Another drawback of robust sliding mode control is that it requires system model information and error bounds on disturbances. Which could be difficult to formulate during uncertain conditions while performing obstacle avoidance maneuvers. To help mitigate some of these shortcomings, this research proposes to use a virtual particle in concert with artificial potential functions to define a reference trajectory. The reference trajectory will then be tracked by the actual spacecraft via a direct adaptive controller to provide smooth tracking. The cases of both static and dynamics obstacles are considered for arbitrary initial conditions. By separating the task of path planning to avoid obstacles from the actual system dynamics, the problem of tracking a potential field for obstacle avoidance is significantly simplified, and results in less complicated control architecture. The reference trajectory for the spacecraft is generated in real-time with the system dynamics. Obstacle avoidance and convergence to the goal position in finite time are achieved.

SPACECRAFT DYNAMICS MODEL

The spacecraft is assumed to be in orbit around earth in a reference orbit at an altitude of 500km. The dynamics of the spacecraft is given using the Clohessy-Wiltshire relative motion equations as in Eq. (1 - 3)¹⁰⁻¹¹. Disturbances are added to the spacecraft in the form of force inputs F_d . For scenarios with a disturbance, sinusoidal disturbances are considered in all three axes.

$$\ddot{x} = 2n\dot{y} + 3n^2x + u_x + F_{dx} \quad (1)$$

$$\ddot{y} = -2n\dot{x} + u_y + F_{dy} \quad (2)$$

$$\ddot{z} = -n^2z + u_z + F_{dz} \quad (3)$$

Where, u_i are the thrust control inputs, F_{di} are the disturbance forces for $i = x, y, z$ and $n = \sqrt{\frac{\mu}{R_0^3}}$, is the mean orbital rate of the circular target orbit, and finally (x, y, z) are the local Cartesian coordinates of the spacecraft in the relative frame.

The system can be expressed in the state-space form as

$$\begin{aligned}\dot{\mathbf{x}} &= \mathbf{A}\mathbf{x} + \mathbf{B}\mathbf{u} + \mathbf{F}, & \mathbf{x} &\in R^6 \\ \mathbf{y} &= \mathbf{C}\mathbf{x} & \mathbf{y} &\in R^3\end{aligned}\quad (4)$$

where \mathbf{A} , \mathbf{B} and \mathbf{C} are given as

$$\mathbf{A} = \begin{bmatrix} 0 & 0 & 0 & 1 & 0 & 0 \\ 0 & 0 & 0 & 0 & 1 & 0 \\ 0 & 0 & 0 & 0 & 0 & 1 \\ 3n^2 & 0 & 0 & 0 & 2n & 0 \\ 0 & 0 & 0 & -2n & 0 & 0 \\ 0 & 0 & -n^2 & 0 & 0 & 0 \end{bmatrix}, \mathbf{B} = \begin{bmatrix} \mathbf{0}_{3 \times 3} \\ \mathbf{I}_{3 \times 3} \end{bmatrix}, \mathbf{C} = [\mathbf{I}_{3 \times 3} \quad \mathbf{I}_{3 \times 3}] \quad (5)$$

It can be noted that \mathbf{C} outputs the combination of position and velocity, also known as sensor blending. The external disturbance \mathbf{F} is modelled as a sinusoidal disturbance and applied to each axis. The system and disturbance model is unknown to the adaptive controller.

The disturbance is given as

$$\mathbf{F} = \begin{bmatrix} 0 \\ 0 \\ 0 \\ \sin(0.04(t + \pi/2)) \\ \sin(0.01 * (t + \pi)) \\ \sin(0.02 * t + 2 * \pi) \end{bmatrix} \times 10^{-4} \text{ m/s}^2 \quad (6)$$

ARTIFICIAL POTENTIAL FUNCTIONS

In this section the model for the artificial potential fields used for the reference trajectory path planning are defined. Both attractive and repulsive potential fields are utilized to produce a trajectory that reaches the goal locations while avoiding all obstacles. Because potential field functions are scalar additive functions, a total potential field is found by simply adding the contributions of the attractive potential, and all repulsive potentials. For convenience we can define every obstacle (debris piece) to have it's own repulsive potential. Define $U_{att}(\mathbf{r})$ to be the attractive potential from the goal location felt at point \mathbf{r} and $U_{rep_i}(\mathbf{r})$ to be the repulsive potential felt at point \mathbf{r} in response to obstacle i (where $i = 1, 2, \dots, N$ up to the number of obstacles). Equations (7) and (9) give the attractive and repulsive potential functions respectively. Note that the repulsive potential is set to 0 beyond a chosen safety radius, d_0 , beyond which the obstacle can be safely ignored. By enforcing a minimum distance before feeling repulsive potentials, avoidance of obstacles is achieved without complicating calculations for obstacles whose potential function would be very small at high distances.

$$U_{att}(\mathbf{r}) = \frac{1}{2}(\mathbf{r} - \mathbf{r}_{goal})^T K_{att}(\mathbf{r} - \mathbf{r}_{goal}) \quad (7)$$

$$U_{rep_i} = \frac{1}{2}K_{obst_i} \left(\frac{1}{d_{obst_i}} - \frac{1}{d_0} \right) \quad \text{if } d_{obst_i} \leq d_0 \quad (8)$$

$$U_{rep_i} = 0 \quad \text{if } d_{obst_i} > d_0 \quad (9)$$

The force felt by the virtual point can be found by taking the negative gradient of the potential functions. Thus the attractive force takes the form of a simple spring force as shown in equation (10). The farther from the goal point, the larger the force applied to the virtual particle to pull it towards the goal position.

$$\mathbf{F}_{att} = -\nabla U_{att} = -k_{att}(\mathbf{r} - \mathbf{r}_{goal}) \quad (10)$$

Similarly, the repulsive force is found from the negative gradient of the repulsive potential. Note that just as the potential is only felt inside a safety radius d_0 , so the repulsive force will only be felt if the virtual particle is within the safety radius. The repulsive force for each obstacle is defined as:

$$\mathbf{F}_{rep_i} = -\nabla U_{rep_i} \quad (11)$$

$$\mathbf{F}_{rep_i} = k_{obst_i} \left(\frac{1}{d_{obst_i} - \frac{1}{d_0}} \right) \quad (12)$$

$$\frac{1}{d_{obst_i}^2} \frac{\mathbf{r} - \mathbf{r}_{obst_i}}{d_{obst_i}} \quad \text{if } d_{obst_i} < d_0 \quad (13)$$

$$\mathbf{F}_{rep_i} = 0 \quad \text{if } d_{obst_i} > d_0. \quad (14)$$

The additive property of scalar potential functions allows arbitrary numbers of potential functions to be combined into one total potential force field. The total potential field for the virtual particle is given by as the sum of the attractive and all repulsive potentials as shown in equation (15).

$$U_{total} = U_{att} + \sum_{i=1}^{N_{obs}} U_{rep_i} \quad (15)$$

The total force applied to the virtual system will result from the gradient of the total potential function shown in equation (16).

$$\nabla U_{total} = \nabla U_{att} + \sum_{i=1}^{N_{obs}} \nabla U_{rep_i} \quad (16)$$

The virtual system dynamics are defined by a gradient steepest descent algorithm. Repulsive potentials are defined as positive, while attractive potentials are defined as negative. Seeking the lowest point of the total potential function U_{total} gives a path that avoids all obstacles. Define the virtual system's position to be $\mathbf{x}_v \in \mathbb{R}^3$, then the iteration to find the minimum of the potential function is given by equation (17). The initial condition \mathbf{x}_{v_0} is taken to be the initial position of the spacecraft, \mathbf{X}_0 .

$$\mathbf{x}_v(i+1) = \mathbf{x}_v(i) - \alpha \nabla U_{total} \quad (17)$$

Where $\alpha > 0$ controls the rate of convergence by acting as the current step size in the direction of greatest descent. Note that if desired, α can be constant or change in size to provide steps of equal size during the gradient descent process. After each iteration, the virtual particle's position is updated. While the virtual system is running, a virtual "velocity" is calculated as a vector in the current direction of greatest descent as shown in equation (18).

$$\dot{\mathbf{x}}_v = \frac{\nabla U_{total}}{\|\nabla U_{total}\|} \quad (18)$$

Combined with the virtual particle positions, a complete reference trajectory consisting of $[\mathbf{x}_v^T \dot{\mathbf{x}}_v^T]^T \in \mathbb{R}^6$ is now fully defined for the spacecraft to track. The approach outlined thus far works ideally for generating a smooth trajectory that avoids obstacles and reaches the goal point. However, in order to smoothly descend to the final position, the spacecraft trajectory generation for the final few meters is switched to an exponentially decaying reference trajectory to the goal position.

DIRECT ADAPTIVE CONTROLLER

A model reference direct adaptive controller is implemented in this paper based on the simple adaptive control (SAC) strategy.¹² The controller doesn't require the system's explicit dynamical model and is capable of robust trajectory tracking under unknown random disturbances. In this paper, the controller follows the reference trajectories generated through the APF and a user defined trajectory as given in the following section.

The form of an direct adaptive controller is followed from Tiwari¹³ and the control is given as

$$\mathbf{u} = \mathbf{K}_e(t)\mathbf{e}_y + \mathbf{K}_x(t)\mathbf{x}_m + \mathbf{K}_u(t)\mathbf{u}_m \quad (19)$$

Here \mathbf{e}_y is the output tracking error defined as

$$\mathbf{e}_y = \mathbf{y}_m - \mathbf{y} \quad (20)$$

$$\mathbf{e}_y = \mathbf{C}\mathbf{x}_m - \mathbf{C}\mathbf{x} \quad (21)$$

where \mathbf{y}_m and \mathbf{y} are the output vectors of the reference and actual models respectively.

$\mathbf{K}_e(t) \in R^{m \times m}$ is the time-varying control gain matrix, $\mathbf{K}_x(t) \in R^{m \times n}$ and $\mathbf{K}_u(t) \in R^{m \times m}$ are time-varying feedforward control gains, and \mathbf{x}_m and \mathbf{u}_m are the states and control vectors of the reference model.

The adaptive gains \mathbf{K}_e , \mathbf{K}_x and \mathbf{K}_u from 19 are given as the summation of integral adaptive gains $\mathbf{K}_I = [\mathbf{K}_{Ie} \ \mathbf{K}_{Ix} \ \mathbf{K}_{Iu}]$ and proportional adaptive gains $\mathbf{K}_P = [\mathbf{K}_{Pe} \ \mathbf{K}_x \ \mathbf{K}_{Pu}]$ as follows:

$$\begin{aligned} \mathbf{K}_e(t) &= \mathbf{K}_{Ie}(t) + \mathbf{K}_{Pe}(t) \\ \mathbf{K}_x(t) &= \mathbf{K}_{Ix}(t) + \mathbf{K}_{Px}(t) \\ \mathbf{K}_u(t) &= \mathbf{K}_{Iu}(t) + \mathbf{K}_{Pu}(t) \end{aligned} \quad (22)$$

It has been shown in¹⁴ that in order to guarantee stability only integral gain is required. However, the addition of proportional gains \mathbf{K}_p improves the rate of convergence and decrease oscillatory effects.

The integral control update law is given as

$$\begin{aligned}
\dot{\mathbf{K}}_{Ie}(t) &= -\mathbf{e}_y(t)\mathbf{e}_y^T(t)\mathbf{\Gamma}_e \\
\dot{\mathbf{K}}_{Ix}(t) &= -\mathbf{e}_y(t)\mathbf{x}_m^T\mathbf{\Gamma}_r \\
\dot{\mathbf{K}}_{Iu}(t) &= -\mathbf{e}_y(t)\mathbf{u}_m^T\mathbf{\Gamma}_u
\end{aligned} \tag{23}$$

Here $\mathbf{\Gamma}_e$, $\mathbf{\Gamma}_r$ and $\mathbf{\Gamma}_u$ are positive definite weighting matrices (tuning parameters) for the integral adaptive control law. It can be noted that these parameters must be manually tuned. Some guidance on how to tune these parameters is provided in Kaufman.¹²

The proportional control update law is given as

$$\begin{aligned}
\mathbf{K}_{Pe}(t) &= -\mathbf{e}_y(t)\mathbf{e}_y^T(t)\bar{\mathbf{\Gamma}}_e \\
\mathbf{K}_{Px}(t) &= -\mathbf{e}_y(t)\mathbf{x}_m^T\bar{\mathbf{\Gamma}}_r \\
\mathbf{K}_{Pu}(t) &= -\mathbf{e}_y(t)\mathbf{u}_m^T\bar{\mathbf{\Gamma}}_u
\end{aligned} \tag{24}$$

Here, $\bar{\mathbf{\Gamma}}_e$, $\bar{\mathbf{\Gamma}}_r$ and $\bar{\mathbf{\Gamma}}_u$ are positive semi-definite matrices used to tune the proportional adaptive gain laws.

A modified form of SAC is applied in this controller as given in Equation (25). This form does not include the feedforward control as the APF does not generate these terms. The stability conditions are presented in our previous work.¹³

The modified adaptive control is then given as

$$\mathbf{u} = \mathbf{K}_e(t)\mathbf{e}_y \tag{25}$$

SIMULATION AND RESULTS

In this section, we present results for a particular scenario.

Proximity Reference Trajectory

As the spacecraft gets closer to the goal point, the spacecraft's speed needs to be gradually reduced. Therefore, a new reference trajectory model is generated in proximity of the goal point as given below. This model ensures a smooth transition from APF generated trajectory to the goal point. The reference also allows for spacecraft hovering at the goal point.

The reference trajectory is given as

$$\mathbf{x}_m = \mathbf{x}_{in}e^{\alpha t^3} + \mathbf{x}_f(1 - e^{\alpha t^3}) \tag{26}$$

$$\mathbf{y}_m = \mathbf{C}\mathbf{x}_m \tag{27}$$

where $\mathbf{y}_m \in R^3$ is the time-varying output equation for the spacecraft to track. The tuning parameter $\alpha = -1 \times e^{-9}$ corresponds to the rate of change of position which can be tuned depending on time constraints. $\mathbf{x}_{in} = [\mathbf{x}_{inp} \ \mathbf{x}_{inv}]$ is the initial position and velocity of the spacecraft and the $\mathbf{x}_f = [\mathbf{x}_{fp} \ \mathbf{x}_{fv}]$ is the final spacecraft goal position and velocity in the hill frame. The reference trajectory from Equation (26) generates a time-varying smooth trajectory for the adaptive controller for tracking. It can be noted here that the direct adaptive controller of the form of Equation (19) requires a time-varying trajectory to track between initial and final states.

Simulation Properties

The debris avoidance scenarios and simulation results are presented in this section. Common scenario parameters such as the spacecraft mass and reference orbit are shown in Table 1.

Table 1: Common Scenario Parameters

Parameter	Value	Unit	Description
R_0	6878	km	Reference orbit radius
m_0	500	kg	Spacecraft mass
k_{rep}	50		Repulsive Potential Gain
k_{att}	0.011		Attractive Potential Gain
r_{safe}	20	m	Safety Radius

The initial condition and final condition for the spacecraft is given as

$$\begin{aligned} \mathbf{x}_{p0} &= [20 \ 20 \ 0]^T \text{ m}, \quad \mathbf{x}_{v0} = [-0.0707 \ -0.0707 \ 0]^T \text{ m/s} \\ \mathbf{x}_{pf} &= [0 \ 0 \ 0]^T \text{ m}, \quad \mathbf{x}_{vf} = [0 \ 0 \ 0]^T \text{ m/s} \end{aligned} \quad (28)$$

It can be noted that the initial conditions for the reference trajectory given in Equation (26) is simply the final conditions from the APF. The integral adaptive gains are initialized with zero initial condition. The adaptive tuning parameters are given as $\mathbf{\Gamma}_e = \bar{\mathbf{\Gamma}}_e = 10 I_{3 \times 3}$.

Table 2 gives the positions of the obstacles for the scenario in local Cartesian coordinates. Thirteen obstacles were placed between the spacecraft initial position and the goal position such that no straight line path (the easiest path) would exist to the goal position. Note that the obstacles are considered static for this case so that the spacecraft must perform an avoidance maneuver to avoid a collision.

Table 2: Obstacle Positions

r_{obs_x}	10	10	-5	1	-3	-4	-6	-1	2	4	8	6	7
r_{obs_y}	8	12	0	5	8	6	3	10	4	5	7	9	13
r_{obs_z}	0	0	0	0	0	0	0	0	0	0	0	0	0

Simulation Results

This section presents the results for two scenarios: (a) system model without disturbances and (b) system model with sinusoidal disturbances added to all axes of the spacecraft. Figure (1) and (2) shows the spacecraft trajectory in 3D space for scenarios (a) and (b). Trajectory results show that the APF can generate an obstacle avoidance path and the adaptive control successfully tracks the reference trajectory generated with APF resulting in obstacle avoidance and convergence to the goal location in finite time. Due to the disturbances in scenario (b), the adaptive controller rejects the unknown disturbances and achieves successful tracking of the reference trajectory as before. However, the spacecraft displaces slightly before the adaptive control restores the spacecraft on the reference trajectory as evidenced in the movement seen in the z-axis of the 3D trajectory shown in Figure (2) and the time position trajectory shown in Figure (4 (a)).

Figures (3(a)) and (4(a)) show the spacecraft's position with time and it can be seen that the spacecraft successfully converges to the goal position. Note that when an obstacle is at a distance the spacecraft heads directly towards the goal, but when an obstacle approaches too close the spacecraft maneuvers to avoid a collision and continue heading towards the goal location. Figures (3(b)) and (4(b)) shows the plots for the velocity profiles of the spacecraft. The magnitude of the velocity is kept constant at 0.05 m/s until the trajectory is switched to the final convergence trajectory.

Figures (3 (c)) and (4(c)) shows the control effort generated by the adaptive control system. The spike (~ 1450 sec) is due to the switching from the APF trajectory to the user-defined trajectory as given in Equation (26). This spike can be further reduced depending on the velocity commands. The maximum control effort generated is constrained to 0.004 m/s^2 (which corresponds to a control force of 2N given the spacecraft assumed mass). In scenario (b), the adaptive control can successfully generate a disturbance rejection control effort, as shown in Figure (4(c)). Unlike scenario (a), a non-zero control effort is required after reaching the goal position to counter the disturbances.

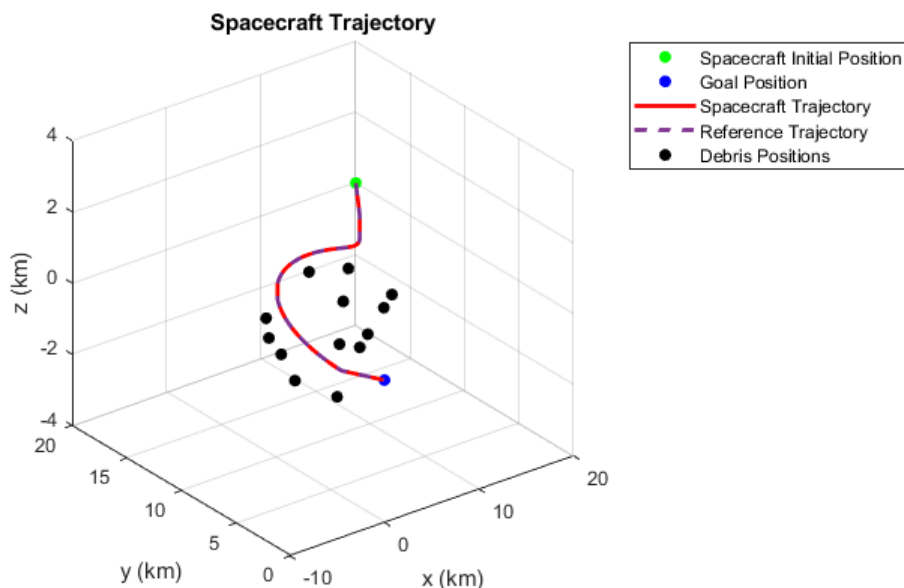


Figure 1: Satellite 3D position without disturbances

CONCLUSION

The model-free APF architecture is able to generate obstacle avoidance reference trajectories in the presence of dynamic and static obstacles. Furthermore, the adaptive controller is shown to successfully track the generated trajectories and maintain a safe distance from all obstacles. Disturbance rejection from the model was also achieved and shows one of the key advantages of using an adaptive control architecture. Future work involves using adaptive potential functions and modeling the spacecraft and debris with full two-body non-linear dynamics and disturbances.

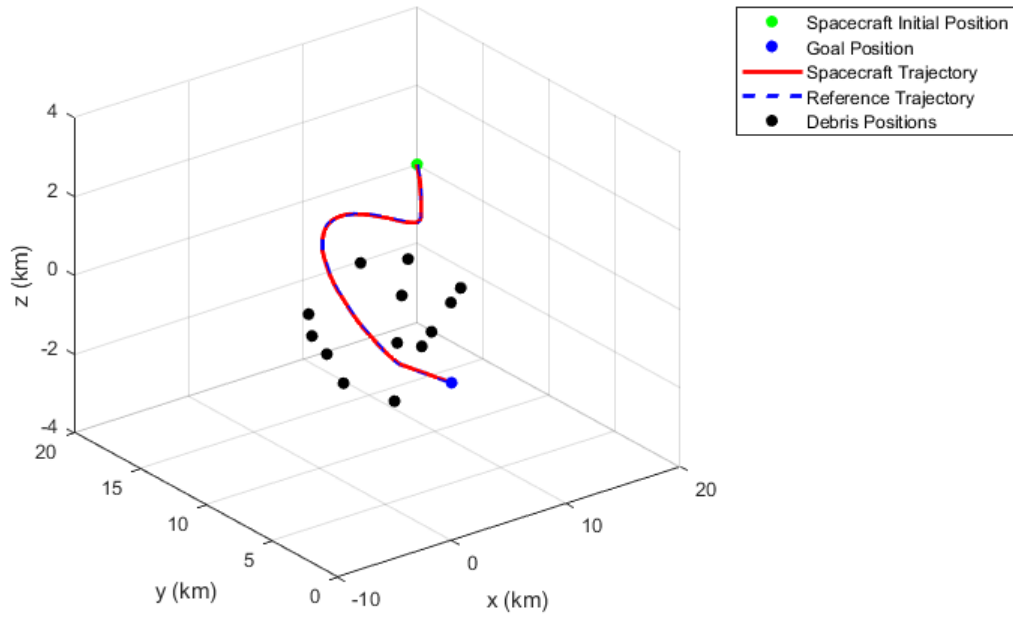


Figure 2: Satellite 3D position with disturbances

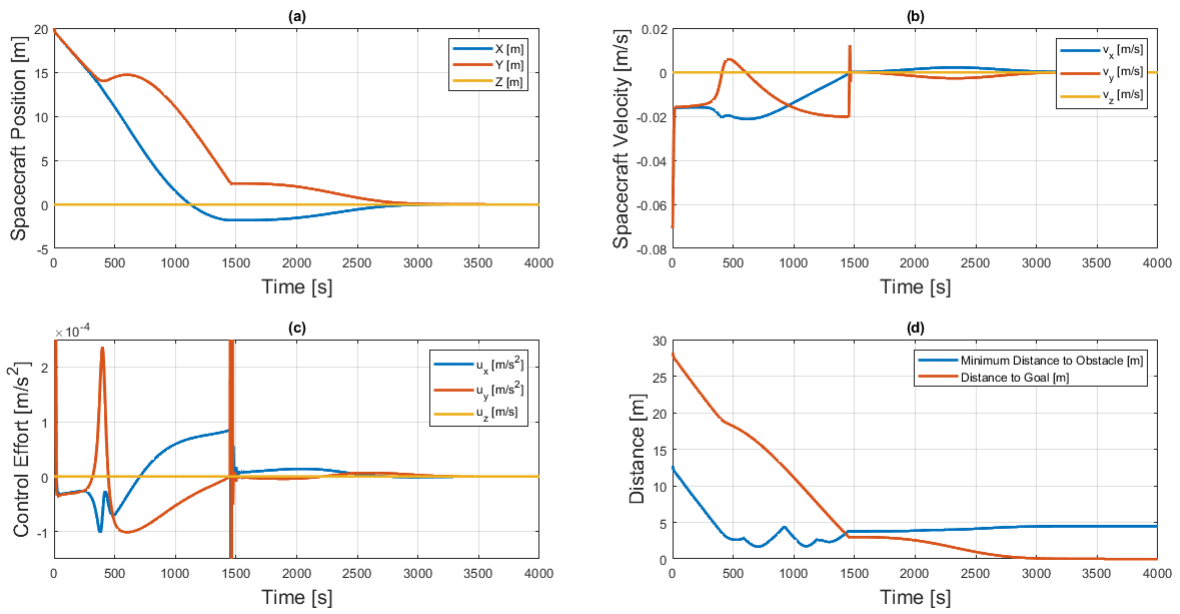


Figure 3: Simulation results: (a) spacecraft position, (b) spacecraft velocity, (c) control effort, and (d) distance from obstacles and goal.

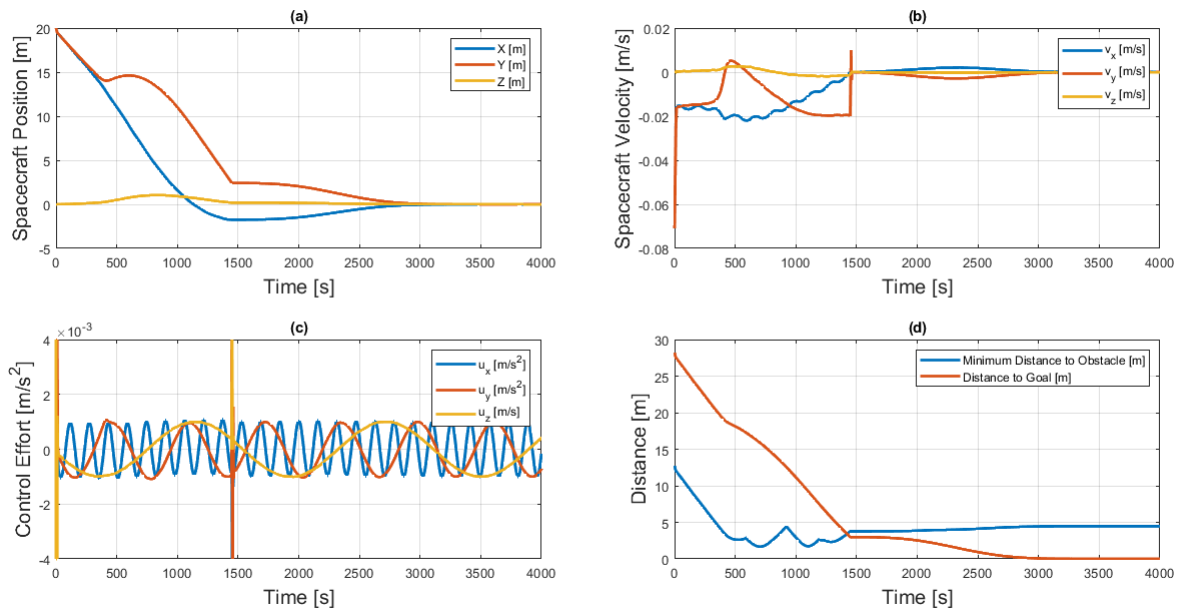


Figure 4: Simulation results with sinusoidal disturbances in all axes: (a) spacecraft position, (b) spacecraft velocity, (c) control effort, and (d) distance from obstacles and goal.

REFERENCES

- [1] N. L. Johnson, "Orbital Debris: the Growing Threat to Space Operations," Feb. 2010.
- [2] M. Hülsmann, R. Kahle, M. Schneller, S. Aida, M. Hahn, E. Panzenböck, A. Spörl, T. Terzibaschian, and W. Halle, "Debris collision avoidance by means of attitude control-in-flight demonstration with TET-1," *Journal of Space Safety Engineering*, Vol. 6, Dec. 2019, pp. 284–290.
- [3] S. Omar, "Spacecraft Collision Avoidance Using Aerodynamic Drag," *J. Guid. Control Dyn.*, Vol. 43, No. 3, pp. 567–573.
- [4] J. Guldner and V. I. Utkin, "Sliding mode control for gradient tracking and robot navigation using artificial potential fields," *IEEE Trans. Rob. Autom.*, Vol. 11, Apr. 1995, pp. 247–254.
- [5] Nicoletta Bloise, Elisa Capello, Matteo Dentis, and Elisabeth Punta, "Obstacle Avoidance with Potential Field Applied to a Rendezvous Maneuver," *applied sciences*, Oct. 2017.
- [6] Nicoletta Bloise, Elisa Capello, Matteo Dentis, and Elisabeth Punta, "Obstacle Avoidance with Potential Field Applied to a Rendezvous Maneuver," *applied sciences*, Oct. 2017.
- [7] Q. Li, J. Yuan, and H. Wang, "Sliding mode control for autonomous spacecraft rendezvous with collision avoidance," *Acta Astronaut.*, Vol. 151, Oct. 2018, pp. 743–751.
- [8] Q. Li, J. Yuan, B. Zhang, and H. Wang, "Artificial potential field based robust adaptive control for spacecraft rendezvous and docking under motion constraint," *ISA Trans.*, May 2019.
- [9] L. Cao, D. Qiao, and J. Xu, "Suboptimal artificial potential function sliding mode control for spacecraft rendezvous with obstacle avoidance," *Acta Astronaut.*, Vol. 143, Feb. 2018, pp. 133–146.
- [10] B. Wie, *Space Vehicle Dynamics and Control, Second Edition*. AIAA Education Series, American Institute of Aeronautics and Astronautics, Jan. 2008.
- [11] H. Schaub and J. L. Junkins, *Analytical mechanics of space systems*. Reston, VA: American Institute of Aeronautics and Astronautics, Inc., 2003.
- [12] H. Kaufman, I. Barkana, and K. Sobel, *Direct Adaptive Control Algorithms: Theory and Applications*. Springer Science & Business Media, Nov. 1997.
- [13] M. Tiwari, R. J. Prazenica, and T. Henderson, "Tracking Reference Orbits Around Asteroids with Unknown Gravitational Parameters Using a Nonlinear Adaptive Controller," *AIAA Scitech 2020 Forum*, AIAA SciTech Forum, American Institute of Aeronautics and Astronautics, Jan. 2020.
- [14] I. Barkana, "Output feedback stabilizability and passivity in nonstationary and nonlinear systems," *Int. J. Adapt Control Signal Process.*, Vol. 22, 2010.